Progressive Collapse Resisting Mechanisms of Planar Prestressed Concrete Frame

Kai Qian, Xi-De Zhang, Feng Fu, and Bing Li,

Biography:

ACI member **Kai Qian** is a Research Fellow at Nanyang Technological University, Singapore. He received his MSC and PhD degrees from Nanyang Technological University, Singapore. His research interests include reinforced concrete and prestressed concrete structures design, particularly in the area of progressive collapse and blast resistance.

Xi-De Zhang is a Professor in the College of Civil Engineering and Architecture at Guangxi University, Nanning, China. His research interests include reinforced concrete and composite structures design, particularly in the area of seismic resistance.

ASCE Member Feng Fu is a Lecturer in Structural Engineering, City, University of London, U.K. and Changbai Mountain distinguished professor, Jilin Jianzhu University, Jilin, China. His research interests include finite element simulation on RC and composite structures, particularly in the area of progressive collapse and blast resistance. He is a Member of Disproportionate Collapse Mitigation of Building Structure Standards and Member of Blast Protection of Building Standard, American Society of Civil Engineers

ACI member **Bing Li** is an Associate Professor in the School of Civil and Environmental Engineering at Nanyang Technological University, Singapore. He received his PhD degree from the University of Canterbury, Christchurch, New Zealand. He is a member of ACI Committee 377, Performance-Based Structural Integrity and Resilience of Concrete Structures, and Joint ACI-ASCE Committees 352, Joints and Connections in Monolithic Concrete Structures, and 441, Reinforced Concrete Columns (corresponding author).

ABSTRACT

The paper presents the behavior of six tests of Planar Prestressed Concrete Frame under the

loss of a middle column. The six tests consist of two non-prestressed reinforced concrete (RC) specimens and four prestressed concrete (PC) specimens with bonded post-tensioning tendons (BPT). The structural response of the specimens with different flexural reinforcement ratio, span/depth ratio, and effective prestress level has been reported. In addition, the impact of parabolic BPT on the behavior of RC frames to resist progressive collapse is also evaluated. Experimental results indicated that the BPT can not only increase the initial stiffness and yielding load of the RC counterparts, but also increase the ultimate load capacity in the catenary action stage. Moreover, it will impact the load resisting mechanisms and the failure modes. Contrary to the commonly accepted sequential mobilization of compressive arch action and catenary action to resist progressive collapse of RC frames, no effective compressive arch action is developed in PC frames to mitigate progressive collapse risk. Based on experimental observations, it is found that higher effective prestress in BPT results in enhanced initial stiffness and yielding load but less deformation capacity and ultimate load capacity. It is also found that higher non-prestressed flexural tensile reinforcement ratio could improve the behavior of PC specimens to resist progressive collapse.

Keywords: progressive collapse; prestressed concrete; compressive arch action; catenary action; mechanism; bonded; post-tensioning tendon.

INTRODUCTION

Progressive collapse is defined as "the spread of an initial local failure from element to element, which eventually results in the collapse of an entire structure or a disproportionately large part of it"[1]. As the accidents or terrorist attacks are unpredictable, conventional civil structures cannot be risk-free. Thus, one of the most popular topics in structural engineering

in the last decade is evaluating the behavior and load resisting mechanism of different types of building structures to mitigate progressive collapse risk. Currently, the commonly used method to evaluate the progressive collapse resistance of structures is based on the remaining structures following initial local failure such as the loss of a load bearing column or partial of walls[2-4]. Alternate load path method is popular used for progressive collapse design[5-9]. Based on alternate load path method, a number of tests[2-11] had been carried out. All foregoing test results[2-11] demonstrated that considerable compressive arch action could enhance the yielding load capacity of reinforced concrete (RC) beams in relatively small deformation stage while catenary action could develop in beam longitudinal reinforcements in large deformation stage. These tests are focused on RC frames and thus, their conclusions may not be able to refer for designing of prestressed concrete (PC) frames to mitigate progressive collapse effectively. As well known, nowadays, PC technique is frequently used in commercial buildings with long spans. Parabolic tendons with drape are commonly installed in the continuous beams to apply pre-compression force in the expected tensile zone, as shown in **Fig. 1a**. However, the bending moment reversal will occur in the beams after removal of the middle column: such as the initial hogging moment in the beam end at the location of the middle column changes to sagging moment after removal of the column, as shown in **Fig. 1b**. If a middle column is removed accidentally, the profile of tendons will differ with the bending moment distribution along the beams. It is well known that the PC frames are shallower in depth than their RC counterparts with the same span and loading conditions. Thus, the PC frames may have higher possibility to trigger progressive collapse when the profile of prestressing tendons deviate its design purpose after accidentally removal of the columns. Therefore, it is imperative to carry out the investigations to capture the behavior of PC frames under the removal of a middle column. However, limited studies, especially experimental tests, have had been conducted on the capacity of PC frames to mitigate

progressive collapse.

The behaviour of PC frame with unbonded post-tensioning (UPT) tendons was investigated by Qian *et al*.[12]. It is well known, for unbonded tendons transfer the force to the concrete via the end anchors and the profile of tendons. However, the force of bonded tendons can be transferred to the concrete through the bond between the tendons and concrete. Thus, the PC frames with bonded tendons may behave quite differently to unbonded tendons[13]. Therefore, the previous work of Qian *et al*.[12] has been extended to carry out a programme of tests on PC beam-column subassemblages with bonded post-tensioning tendons (BPT), which will be presented in this paper.

RESEARCH SIGNIFICANCE

The stress profile of tendons may differ with the bending moment distribution after removal of a middle column, which may result in possible collapse of PC frame. To quantify the possible load resisting mechanisms of PC frames subjected to a middle column missing scenario, a series of four PC beam-column subassemblages with BPT are tested in this study. By comparing to conventional RC subassemblages and PC subassemblages with UPT, the effects on BPT could be evaluated quantitatively. Due to no special provisions in existing guidelines (GSA[14] and DoD[15]) for mitigating the progressive collapse risk of PC frame, the test results may provide necessary research outcome to fill the gap. Moreover, this research extends the availability of benchmarking data for the development of reliable analytical or numerical models as limited test data are available in literature.

EXPERIMENTAL PROGRAM

Test Specimen

Six specimens are designed and constructed to investigate the performance of PC beam-column sub-assemblages with BPT to resist progressive collapse caused by the loss of a

middle column due to blast or vehicular impact. These six specimens include four PC beam-column subassemblages (PCSL-0.6, PCSL-0.75, PCSH-0.6, and PCLL-0.6) and two non-prestressed RC counterparts (RCSL and RCLL). For example, the designation of PCSL-0.6 represents PC specimen with short span (span/depth ratio of 12), low amount of non-prestressed reinforcement, and the effective prestress (f_{pe}) of $0.6f_{pu}$. where f_{pu} is the ultimate strength of the tendon. Similarly, the designation of RCSL represents non-prestressed RC specimen with short span and low longitudinal reinforcement ratio. **Table 1** gives the designation and characteristics of each specimen. The specimens are one-half scaled due to facility capacity in laboratory. The prototype frame of the specimens is located at the middle of a perimeter frame of a six story office building, which has 4.2 m and 3.3 m high in the first and upper story, respectively. The design span is 6 m and 7 m for prototype frame with short and long span, respectively. The RC detail of the specimens are following the seismic design requirement in accordance with ACI 318-14[16] and assumed to be located on a D class site (stiff soil profile) where the design spectral response acceleration parameters, S_{DS} and S_{D1}, are 0.45 and 0.30, respectively. The live load (LL) is assumed to be 2.0 kPa while the dead load (DL) including the self-weight is assumed to be 3.75 kPa. As shown in **Fig. 2**, each specimen comprises of two side columns, one middle column, and two beams. All specimens are half-scaled due to capacity limits of the test facilities. The cross-section of beam and middle column are 150 mm×250 mm (2.9 in.×9.8 in.) and 250 mm×250 mm (9.8 in.×9.8 in.), respectively. However, the size of side column is enlarged to 400 mm×400 mm (15.7 in.×15.7 in.) for applying fixed boundary conditions well. For Specimen PCSL-0.6, the beam non-prestressed reinforcements of 3T10 are installed in both top and bottom layer, which corresponds to reinforcement ratio of 0.7%. The reinforcements are placed in the beam continuously. T10 and R6 herein represent deformed reinforcement with diameter of 10 mm (0.4 in.) and plain reinforcement with diameter of 6 mm (0.2 in.), respectively. As shown in

the figure, a plastic duct with internal diameter of 32 mm (1.3 in.) is installed with parabolic profile before casting. After erected the specimen in the setup, a tendon with nominal diameter of 12.7 mm (0.5 in.) is threaded through the duct and jacked it to target effective prestress $0.6f_{pu}$. Following that, grouting is conducted immediately. To ensure effective bonding between BPT and concrete, each specimen is tested after grouting over least three days. The true effective prestress of BPT deducting the prestress loss are measured and tabulated in **Table 1**. The tendon is twisted by seven high-strength wires with nominal area of 98 mm^2 (0.2 in^2.). The parabolic profile of the tendon is following Eqs. 1 and 2.

$$y_1 = 0.12x_1^2 \quad (1)$$

$$y_2 = 0.28x_2^2 \quad (2)$$

where y_1 is the vertical coordinate of the tendon from the origin in the middle of the beam, x_1 is the horizontal coordinate of the tendon from the origin in the middle of the beam, y_2 is the vertical coordinate of the tendon from the origin in the middle of the center column, and x_2 is the horizontal coordinate of the tendon from the origin in the middle of the center column.

PCSL-0.75 has identical dimensions and reinforcement details as PCSL-0.6 but higher designated effective prestress $0.75f_{pu}$. Comparing to PCSL-0.6, PCSH-0.6 has higher non-prestressed reinforcement ratio. In PCSH-0.6, the top and bottom beam longitudinal reinforcement are 3T12 in accordance with reinforcement ratio of 1.0 %. For PCLL-0.6, it has similar cross-section and reinforcement details as PCSL-0.6. However, it has longer design span of 3500 mm (137.8 in.) and larger span/depth ratio of 14, as shown in **Fig. 2c**. For comparison easily, two non-prestressed RC specimens (RCSL and RCLL) without BPT are also cast and tested. Specimens RCSL and RCLL have similar dimensions and reinforcement details as the corresponding PC Specimens PCSL-0.6 and PCLL-0.6, respectively.

Based on compressive cylindrical tests, the measured concrete compressive strength of

RCSL, RCLL, PCSL-0.6, PCSL-0.75, PCSH-0.6, and PCLL-0.6 are 44 MPa (6 kip), 44 MPa (6 kip), 45 MPa (6 kip), 44 MPa (6 kip), 45 MPa (7 kip), and 43 MPa (6 kip), respectively. Furthermore, based on tensile splitting tests, the tensile strength of the concrete of RCSL, RCLL, PCSL-0.6, PCSL-0.75, PCSH-0.6, and PCLL-0.6 are 3.1 MPa (0.4 kip), 3.3 MPa (0.5 kip), 3.0 MPa (0.4 kip), 3.5 MPa (0.5 kip), 3.1 MPa (0.4 kip), and 3.4 MPa (0.5 kip), respectively. The properties of reinforcements and strands are tabulated in **Table 2.**

Test setup and instrumentation

Similar to previous tests[2-5], as shown in **Fig. 3**, the side column is substituted with fixed boundary conditions by two horizontal constraints and a pin support. To eliminate the redundant horizontal constraints from the pin support, a series of steel rollers are mounted below it. A hydraulic jack (lower jack) is installed below the middle column stub to release of the axial force manually. The stroke of the jack is initially protruded out to touch the bottom of the middle column stub for simulation of the ground middle column intact. Then, six steel weight assemblages with weight of 5000 kg (11.0 klb) are hung below the beams to simulate the design service load (DL+LL). Once the weights are hung completely and the instrumentations are ready to record data, the stroke of the lower jack is retracted gradually to release its axial force slowly. If the specimen could stabilize after the stroke of the lower jack detaches from the bottom of the middle column stub completely, the stroke of upper jack begins to protrude out to apply additional concentrated force on the middle column until collapse. To eliminate the out-of-plane failure of the two-dimensional (2D) beam-column sub-assemblages, a special designed steel assembly is installed underneath the upper jack. The steel assembly is consisted of a steel box and several steel pins to only allow vertical movement of the middle column but constraints its rotation and horizontal movements. A series of displacement transducers and load cells are installed to monitor the behavior of the specimens. As shown in **Fig. 3b**, load cell #3 is utilized to measure the axial force in the

lower jack. Load cells #1 and #2 are used to measure the applied additional concentrated force from upper jack. Moreover, the vertical load redistribution is measured by the load cells #4 and #5. To monitor the variation of prestressing force in the tendon, load cell #6 is installed at the jacking end. Tension/compression load cells are installed in the horizontal constraints to measure the horizontal reaction applied on the side columns. Displacement transducers D1 to D7 are installed to measure the variation of the deformation shape of the beam. Before casting, strain gauges are installed in the non-prestressed reinforcement and tendons to monitor the local behavior of the specimens.

TEST RESULTS

Global behavior

RC Specimens- for RCSL, as previously mentioned, firstly, the lower jack protruded out to simulate the middle column intact. Then, six steel assemblies with total weights of 5000 kg (11.0 klb) are hung below the beams symmetrically. Thus, the vertical reaction force of -25 kN (-5.6 kip) is measured by the load cell #3 after the weights are hung completely. As shown in **Fig. 4a**, the stage O'A' represents the phase of axial force releasing in the lower jack. It can be seen that the frame structure is still within elastic range when point A' is reached, which is corresponding to a vertical displacement of 34 mm (1.3 in.). Due to bending moment reversal, the cracks in the beam end vicinity of the middle column (BEVM) are formed in the lower part of the section. After that, additional load is applied gradually from the upper jack until the specimen collapse. To facilitate the comparison of the performance, the load-displacement curves are shifted from [0,-25 kN (-5.6 kip)] to origin (0, 0). Take Specimen RCSL as an example, the stage O'A' is shifted to OA. The load-displacement relationship of remaining specimens shown in the figure is after shifting. The critical values described below and listed in **Table 3** are also picked from the shifted curves. From the shifted curve, when the vertical displacement reached 40 mm (1.6 in.), plastic

hinges are formed in the beam. Further increasing the vertical displacement, the load resistance keeps increasing. This is attributed to compressive arch action developed in the beams, as shown in **Fig. 5a**. When the beam ends have sufficient horizontal constraints, the developed compressive struts could distribute partial of the vertical load to the side column directly. The first peak load of the specimen is measured to 44 kN (9.9 kip) at a vertical displacement of 67 mm (2.6 in.). The load resisting capacity began to decrease after this loading stage and severe concrete crushing occurred in the compressive zone. The re-ascending of the load-displacement curve is observed when the vertical displacement is beyond 172 mm (6.8 in.). The re-ascending is attributed into catenary action developed in beam longitudinal reinforcements (refer to **Fig. 6a**), although the concrete crushing and flexural cracks are very severe in this stage. Even though rebar fracture subsequently occurred in the beam ends, the load resistance continues increasing until the vertical displacement reached 598 mm (23.5 in.). At this stage, the ultimate load capacity of 68 kN (15.3 in.) is measured and the load resistance is suddenly dropped due to rebar fracture occurred in both beam ends near to the side column (BENS). The failure mode of the specimen is illustrated in **Fig. 7a**. As shown in the figure, rebar fracture is only occurred in the BENS. The two-span beam is deformed as parabolic curve and thus, curved catenary action is developed.

For Specimen RCLL, as it has much larger span/depth ratio, heavier steel weights of 6000 kg (13.2 klb) are designed. Thus, it results in larger initial axial force of -30 kN (6.7 kip) in the lower jack. As shown in the shifted curve, plastic hinges are formed in the beam when the vertical load reached 25 kN (5.6 kip), which means that the yielding load of this specimen is less than the initial axial force. If no other load resisting mechanisms could be employed to resist the vertical load, the specimen would have collapsed during the phase of axial force releasing. Fortunately, the first peak load of 36 kN (8.1 kip) is achieved in this

specimen due to compressive arch action developed in beams, which is greater than its initial axial force (30 kN or 6.7 kip). After that, the load resistance begins to decrease due to concrete crushing. When the vertical displacement reached 120 mm (4.7 in.), the displacement suddenly increased to 273 mm (10.7 in.) caused by the compressive arch action vanished, which result in the load resisting capacity less than the force transferred from the hung steel weights. However, the collapse is prevented at a vertical displacement of 273 mm (10.7 in.) due to the additional load resistance from the catenary action. Thus, the response of this specimen demonstrated that the compressive arch action is the frontier of the defense while the catenary action is the second one. The failure mode of this specimen is shown in **Fig. 7b**. Similar to RCSL, rebar fracture is only observed in BENS and the beams are deformed curved.

PC Specimens-for PCSL-0.6, it has BPT with designed and true effective prestress of $0.6f_{pu}$ and $0.53f_{pu}$, respectively. Similar to RCSL, the initial axial force in the lower jack is about -25 kN (-5.6 kip) after the weight of 5000 kg (11.0 klb) is fully hung. Different with RCSL, no cracks are observed in the beams when the weights are applied. As shown in **Fig. 4b**, the yielding load of 42 kN (9.4 kip), which is 131% of RCSL, is obtained at a vertical displacement of 41 mm (1.6 in.). At this stage, the flexural cracks at the BEVM are wider than that at the BENS, which is quite different with that in RCSL. Additionally, as the load resistance keeps increasing with further increase of the vertical displacement, the value of first peak load is hard to mark. The discussion of the load resisting mechanism in following section will reveal that less compressive arch action is developed in PC beams but the stretching of the tendon will provide additional resistance. When the displacement reached 480 mm (18.9 in.), rebar fracture first occurred in the left BEVM. With the further increase of the displacement to 560 mm (22.0 in.) and 621 mm (24.4 in.), rebar fractures are also observed in the BENS. The ultimate load capacity in catenary action stage is measured to 127

kN (28.5 kip), which is 187% of that of RCSL. Thus, BPT could increase the ultimate load capacity significantly. The test stopped at a vertical displacement of 679 mm (26.7 in.) due to anchor slip occurred in the jacking end. The failure mode of this specimen is shown in **Fig. 8**. Different to RCSL, the PC beams with BPT deformed straightly and the widest crack is formed in the BEVM. Moreover, comparing to RCSL, the crack width in the BENS is much thinner.

Similar to RCLL, PCLL-0.6 has span/depth ratio of 14 and thus, the initial axial force is -30 kN (6.7 kip). The true effective prestress of the tendon is $0.55f_{pu}$ due to prestress loss. The measured vertical displacement is 33 mm (1.3 in.) when the axial force fully released. The yielding load of this specimen is 37 kN (8.5 kip), which is 148% of that of RCLL, at a vertical displacement of 45 mm (1.8 in.). Thus, comparing to PCSL-0.6, BPT is more effective for upgrading the yielding load of RCLL. Similar to PCSL-0.6, hard to mark first peak load in the curve as the load-displacement curve also keeps increasing with increase of the vertical displacement. Rebar fracture is firstly observed in the BEVM at a vertical displacement of 452 mm (17.8 in.). When the vertical displacement reached 550 mm (21.7 in.), rebar fracture is also occurred in the left BENS. The failure mode of this specimen is illustrated in **Fig. 9**. Similar to PCSL-0.6, the beams are deformed straightly. Different to RCLL, more severe damage is occurred in the BEVM than that in BENS.

Comparing to PCSL-0.6, PCSH-0.6 has higher beam longitudinal reinforcement ratio of 1.0%. The vertical displacement is 14 mm (0.6 in.) when the initial axial force in the lower jack is released completely. The yielding load of 55 kN (12.3 kip) is achieved at a vertical displacement of 43 mm (1.7 in.). Thus, comparing to PCSL-0.6, PCSH-0.6 achieved much higher initial stiffness and yielding load. Similar to foregoing PC specimens, the load resistance increases with further increasing the displacement, although concrete crushing and wide cracks are accompanied. The load resistance first drops when the vertical displacement

reached 445 mm (17.5 in.) due to rebar fracture occurring in the right BEVM. Rebar fracture is also observed in the left BENS at a displacement of 613 mm (24.1 in.). The measured ultimate load capacity is 145 kN (32.6 kip), which is about 114% of that in PCSL-0.6.

Comparing to PCSL-0.6, PCSL-0.75 has larger designed effective prestress of $0.75f_{pu}$ and the true effective prestress of $0.71f_{pu}$. Comparing to other PC specimens, the camber of 3 mm (0.1 in.) in the middle-span of the beam is measured before applying the weights. The vertical displacement is measured to be 19 mm (0.7 in.) after completely releasing of the axial force in the lower jack. Moreover, the yielding load of 46 kN (10.3 kip) is measured at a vertical displacement of 40 mm (1.6 in.). Thus, higher initial effective prestress will increase the initial stiffness slightly. The rebar fracture is first occurred in the right BENM at a vertical displacement of 361 mm (14.2 in.), which is much earlier than that in PCSL-0.6. Subsequently, it occurred in the both BENS at the displacements of 490 mm (19.3 in.) and 524 mm (20.6 in.), respectively. The specimen is stopped at a vertical displacement of 575 mm (22.6 in.) due to anchor slipped occurred in the jacking point, similar to PCSL-0.6. The failure mode of PCSH-0.6 and PCSL-0.75 are shown in **Figs. 10** and **11**, respectively.

Horizontal reaction

As shown in **Fig. 12**, for RCSL, considerable compressive force is measured at the lower roller initially. It begins to decrease after vertical displacement reached 100.6 mm (4.0 in.) due to concrete crushing. Tensile force is measured in the lower roller when the vertical displacement reached 487.5 mm (19.2 in.). However, the upper roller consistently measured tensile force during test. Thus, the total compressive force in relatively small displacement stage is mainly attributed to the lower roller while the total tensile force in large displacement stage is attributed to both rollers. However, for PCSL-0.6, much larger tensile force is measured in the upper roller from the beginning of the test due to substantial tensile force from BPT. Moreover, although compressive force is also measured in the lower roller, the

maximum compressive force is -65.6 kN (-14.7 kip), which is much less than that of RCSL.

If we look at the total reaction force, similar to previous RC tests[3-11], for RC specimens, significant compressive reaction force is initially measured in the horizontal constraints. As shown in **Fig. 13,** the maximum compressive reaction force of -136 kN (-30.6 kip) and -142 kN (-32.0 kip) are measured in RCSL and RCLL, respectively. The compressive reaction force began to decrease when the displacement beyond 80 mm or 3.1 in. ($0.03l_n$) and 100 mm or 3.9 in. ($0.03l_n$) for RCSL and RCLL, respectively. l_n represents the clear span of the single beam. In accordance with their load resisting behavior, the decrease of the horizontal reaction force related to the compressive arch action vanishing and concrete crushing. When the vertical displacement beyond 220 mm (8.7 in.) [$0.08l_n$ for RCSL and $0.07l_n$ for RCLL], tensile force is measured. The maximum horizontal tensile force in RCSL and RCLL are 153 kN (34.3 kip) and 135 kN (30.3 kip), respectively. However, different with RCSL and RCLL and previously tested RC specimens[3-11], for PC Specimens PCSL-0.6, PCLL-0.6, PCSH-0.6, and PCSL-0.75, no compressive reaction force is observed during the test, which further confirmed less compressive arch action is developed in PC beams. As explained in **Fig. 5b**, the post-tensioning tendon will aggravate the compressive stress at the BEVM but relieve the compressive stress at the BENS. Thus, no effective compressive strut is able to develop in the beams for load redistribution. However, the tensile reaction force remains constant when the vertical displacement reached 70-80 mm (2.8-3.1 in.). The re-ascending of the tensile reaction force is observed in PC specimens with short and long span at the displacements of 170 mm (6.7 in.) and 190 mm (7.5 in.), respectively. With increasing the vertical displacement, the horizontal tensile force keeps increasing. The maximum tensile reaction force measured in PCSL-0.6, PCSH-0.6, PCSL-0.75, and PCLL-0.6 is 291 kN (65.4 kip), 321 kN (72.1 kip), 265 kN (59.6 kip), and 280 kN (62.9 kip), respectively. The lower reaction force measured in PCSL-0.75 is due to anchor slipped occurred in the jacking end at the relatively early vertical

displacement of 575 mm (22.6 in.).

Prestressing force in BPT

Fig. 14 presents the response of prestress force in the tendon versus the vertical displacement. As shown in the figure, the initial prestress force deducting prestress loss is 97 kN (21.8 kip), 100 kN (22.5 kip), 130 kN (29.2 kip), and 101 kN (22.7 kip) in PCSL-0.6, PCSH-0.6, PCSL-0.75, and PCLL-0.6, respectively. It is found that the prestress force increased slowly before the vertical displacements reached 100 mm (3.9 in.) and 150 mm (5.9 in.) for PC specimen with short and long span, respectively. Comparing the response of horizontal reaction force with prestress force in PC specimens, it is hard to explain the increase of tensile reaction force in the initial stage. It is suggested that since bonded tendon is used in this study, the prestress force measured in the jacking end could not represent the variation of the prestress force of the tendon in other places well. When the vertical displacements exceeds 100 mm and 150 mm (5.9 in.) for PC specimen with short and long span respectively, the increase of the prestress force is linear until yielding. Based on the test results, the maximum tensile force in the tendon of PCSL-0.6, PCSH-0.6, PCSL-0.75, and PCLL-0.6 are 192 kN (43.1 kip), 186 kN (41.8 kip), 187 kN (42.0 kip), and 182 kN (40.9 kip), respectively. They are related to prestress stress of 1.05 f_{pu}, 1.02 f_{pu}, 1.03 f_{pu}, and 1.0 f_{pu}, respectively.

Deformation shape of beams

Fig. 15 gives the beam deformation shape of typical RC and PC specimen in accordance with critical stages: the axial force just released, yield load, first peak load, 100 mm (3.9 in.), 200mm (7.9 in.), 300mm (11.8 in.), and ultimate load. As shown in **Fig. 15a**, for RCSL, the deformation shape of beam is curved. In the ultimate load stage, the chord rotation, which is defined as the ratio of displacement in the middle column to the clear span of the beam[15], will slightly over-estimate the rotation of the BESC but significantly under-estimate the rotation in BEVM. This is quite different with that observed in previous tests[2,4,5,6] as the initial service

load is well simulated in this study. For PCSL-0.6, as shown in **Fig. 15b**, the beam is deformed straightly when the displacement is beyond 100 mm (3.9 in.) and severe flexural cracks are formed in the BEVM. In the ultimate load stage, the chord rotation agrees the deformation shape of the beam well, although it is originally defined for non-prestressed RC specimen in existing design guideline[15].

Strain gauge reading

Figs. 16a and **b** show the variation of strain results along beam top and bottom longitudinal reinforcements of PCSL-0.6, respectively. As shown in the figures, similar to non-prestressed RC specimens[4], bending moment reversal is observed at the BEVM after releasing of the initial axial force in the lower jack. Yielding is first occurred in the top reinforcement at the BENS, rather than the bottom reinforcement at the BEVM, which is quite different to the previous non-prestressed RC specimens[4]. Moreover, the compressive strain in the beam longitudinal reinforcements begins to decrease when the vertical displacement is beyond 400 mm (15.7 in.). When the vertical displacement reached 600 mm (23.6 in.), the bottom reinforcement is in tension across the whole span. **Fig. 16c** gives the results of strain gauges attached on the post-tensioning tendons. Due to unknown reason, partial of the strain gauges are faulty before tests. As shown in the figure, initially, all strain gauge read similar value ranged from 4400 με to 4600 με. When the vertical displacement increased, P2 and P3, which are near to the side column, increased their strain dramatically with high slope. However, the increase of remaining strain gauges is relatively very slow. It can be seen that P11 and P12, which nearby the BEVM, suddenly increased abruptly when the vertical displacement is beyond 400 mm (15.7 in.). Actually, as shown in **Fig. 6b**, the tendon at the BEVM will become a straight line when the vertical displacement reached 400 mm (15.7 in.).

ANALYTICAL ANALYSIS AND DISCUSSIONS

Dynamic performance of tested specimens

The scenario of column missing caused by terrorist attacks is considered in this study. The most realistic setup should be designed by removal of the column suddenly. Although quasi-static pushdown test is most commonly used for evaluation of the performance of beam-column substructures mitigating progressive collapse, it is still necessary to assess the dynamic behavior of beam-column substructures. Capacity curve method, which is first proposed by Izzuddin *et al.*[17], is frequently used to predict the dynamic capacity of the substructures based on the measured load-displacement curves (Tsai and Lin[18], and Qian and Li[19]). The capacity curve method is mathematically expressed as:

$$P_{CC}(u_d) = \frac{1}{u_d}\int_0^{u_d} P_{NS}(u)du \quad (3)$$

where $P_{CC}(u)$ and $P_{NS}(u)$ represent the capacity function and the nonlinear static loading estimated at the displacement demand u, respectively.

Fig. 17 shows the dynamic behavior of test specimens. It is found that the dynamic ultimate capacity of RCSL, RCLL, PCSL-0.6, PCSL-0.75, PCSH-0.6, and PCLL-0.6 are 46.7 kN (10.5 kip), 33.2 kN (7.5 kip), 88.0 kN (19.8 kip), 90.8 kN (20.4 kip), 103.8 kN (23.3 kip), and 69.2 kN (10.5 kip), respectively.

De-composite the resistance contribution of axial force and bending moment

For the process of releasing of axial force in the middle column, based on equilibrium and refer to **Fig. 18**, the bending moment (M_L^M), axial force (N_L^M), and shear force (V_L^M) at Section A-A are determined as:

$$M_L^M = V_L L_L - H_t^L(\delta + 0.35) - H_b^L(\delta - 0.35) - G_7 \times 2.0625 - G_6 \times 1.375 - G_5 \times 0.6875 - \frac{1}{2}q \times L^2 \quad (4)$$

$$N_L^M = [(V_L - G_7 - G_6 - G_5)\tan\theta_L^M + H_L]\cos\theta_L^M \quad (5)$$

$$V_L^M = [(V_L - G_7 - G_6 - G_5) - N_L^M \sin\theta_L^M)]/\cos\theta_L^M \quad (6)$$

where V_L is the vertical reaction force measured by load cell #5 in **Fig. 3b**; H_t^L and H_b^L are the horizontal reaction force from upper and lower roller, respectively; G1~G7are the gravitational load of single weight assembly (8.2 kN and 1.8 kip); q is assumed to 0.001kN/mm (0.006kip/in.) for consideration of the self-weights of the beam; $\theta_L^M = \arctan\left(\frac{D_4 - D_5}{0.6875}\right)$ is based on chord rotation of the segment.

Similarly, the bending moment (M_R^M), axial force (N_R^M), and shear force (V_R^M) in the symmetric section of right beam is determined as:

$$M_R^M = V_R L_R - H_t^R(\delta + 0.35) - H_b^R(\delta - 0.35) - G_1 \times 2.0625 - G_2 \times 1.375 - G_3 \times 0.6875 - \frac{1}{2} q \times L^2 \quad (7)$$

$$N_R^M = [(V_R - G_1 - G_2 - G_3)\tan\theta_R^M + H_R]\cos\theta_R^M \quad (8)$$

$$V_R^M = [(V_R - G_1 - G_2 - G_3) - N_R^M \sin\theta_R^M] / \cos\theta_R^M \quad (9)$$

where V_R is the vertical reaction force measured by load cell #4 in **Fig. 3b**; H_t^R and H_b^R respectively are assumed equal to H_t^L and H_b^L, as no load cells are installed for measuring; $\theta_R^M = \arctan\left(\frac{D_4 - D_3}{0.6875}\right)$ is based on chord rotation of the segment.

After that, based on the vertical force equilibrium at the middle joint, it is determined that:

$$P = (N_L^M \sin\theta_L^M + V_L^M \cos\theta_L^M) + (N_R^M \sin\theta_R^M + V_R^M \cos\theta_R^M) \quad (10)$$

After re-arrangement, it becomes:

$$\begin{aligned} P &= (N_L^M \sin\theta_L^M + N_R^M \sin\theta_R^M) + (V_L^M \cos\theta_L^M + V_R^M \cos\theta_R^M) \\ &= \sum_r^{L,R} N_r^M \sin\theta_r^M + \sum_r^{L,R} V_r^M \cos\theta_r^M \end{aligned} \quad (11)$$

where $\sum_r^{L,R} N_r^M \sin\theta_r^M$ and $\sum_r^{L,R} V_r^M \cos\theta_r^M$ represent the resistance contribution from axial force and shear force, respectively. As the shear force could be determined by the bending moment acting on the beams, $\sum_r^{L,R} V_r^M \cos\theta_r^M$ can also be taken as the contribution from the

bending moment. For the process of applying extra axial force on the middle column, the sign of the applied load and shear force will reverse. However, the equations for determination of the internal force are identical. For the sake of brevity, RCSL, PCSL-0.6, and PCSH-0.6 are selected to show the decomposition of vertical resistance.

As shown in **Fig. 19a**, the contribution of shear force begins to decrease after crushing occurred in the beam sections. The re-ascending of the load resisting capacity in catenary action stage is mainly due to the contribution of axial force changing from compression to tension. However, as observed in the figure, before fracture of beam longitudinal reinforcements, shear force (or flexural bending moment) could also provide considerable contribution in the stage of catenary action. Therefore, it is unrealistic to assume the load resisting capacity of the substructures in catenary action stage purely attributed into the tension of beam longitudinal reinforcements, which is commonly accepted by previous studies[20].

As shown in **Fig. 19b**, for PCSL-0.6, the varying of the contribution of shear force is similar to RCSL. However, the contribution of axial force is quite different as the strands could provide considerable tension at the beginning of the test. If we further de-composite the axial force contribution, it is found that compression actually is also observed at the axial force component from RC beam. Moreover, the maximum compression force of 7.5 kN (1.7 kip) is measured in the axial force component from RC beam, which is similar to RCSL. As similar results are observed in PCSH-0.6, no further discussion is given for it.

Effects of span/depth ratio

As shown in **Fig. 4** and **Table 3**, comparing with RCLL, RCSL achieved greater yielding, first peak, and ultimate load by 28%, 22%, and 51%, respectively. However, for PC specimens, the yielding and ultimate load capacity of PCSL-0.6 is about 114% and 122% of that of PCLL-0.6. Thus, the span/depth ratio has greater effects for RC specimens than PC

specimens, especially for ultimate load capacity in catenary action stage. As shown in **Figs. 7**, **8**, and **9**, for both RC and PC specimens, the span/depth ratio has little effects on their failure modes (widest flexural cracks are occurred at the beam end nearby the columns) as the span/depth ratio is 12 and 14 for specimens with short and long design span, respectively. Both span/depth ratios are large enough for flexural dominated failure in beams. Another reason is the prototype frames are seismic designed and detailed, which have high transverse reinforcement ratio in the beam ends nearby the columns and prevented the possible shear failure at the beam end due to smaller span/depth ratio.

Effects of the amount of non-prestressed reinforcements

Comparison of the behavior of PCSL-0.6 and PCSH-0.6, it is found that higher non-prestress reinforcement ratio (1.0%) could increase the yielding load and ultimate load capacity by 31% and 14%, respectively. As listed in **Table 3**, the initial stiffness of PCSL-0.6 and PCSH-0.6 are 0.93 kN/mm (5.3 kip/in.) and 1.23 kN/mm (7.0 kip/in.), respectively. Thus, PCSH-0.6 increased the initial stiffness by 32%. As shown in **Figs. 8** and **10**, the amount of non-prestressed reinforcement ratio has little effects on the failure mode and load resisting mechanism of PC frames to resist progressive collapse. This could be explained as the non-prestressed reinforcement ratio is 0.7% or 1.0% for PC specimens with light or heavy non-prestressed reinforcement, respectively. Similar as above explanation, the relatively heavy transverse reinforcement ratio installed in the beam end nearby the column prevents the possible shear failure even relatively heavy non-prestressed reinforcement ratio is designed.

Effects of the initial effective prestress

Comparing to PCSL-0.6, PCSL-0.75 achieved 10% increase of yielding load. However, PCSL-0.75 exhibited lower ultimate load capacity. This is due to anchor slip occurred in the jacking end at the displacement of 575 mm (22.6 in.), which prevent the tendon to further develop catenary action. As shown in **Figs. 8** and **11**, initial effective prestress has little

effects on the failure mode of the specimen.

Effects of the bonded post-tensioning tendons

By comparing the behavior of PCSL-0.6 with RCSL, it is found that BPT could increase the yielding and ultimate load capacity by 31% and 87%, respectively. For PCLL-0.6, the BPT increased the yielding and ultimate load capacity of RCLL by 48% and 131%, respectively. Thus, BPT has greater impacts on behavior of specimens with larger span/depth ratio. As shown in **Fig. 13**, considerable compressive reaction force is developed in RC beams in the compressive arch action stage, but not PC specimens. This is because little compressive arch action can be developed in PC beams to resist progressive collapse. Comparing the failure mode of PC specimens with corresponding RC specimens, it is found that the BPT will aggravate the damage in the BEVM and relief the damage in the BENS. In PC specimens, rebar fracture is first observed in the BEVM while no rebar fracture is observed in RC specimens, as shown in **Figs. 7**, **8**, and **9**. As shown in **Fig. 6**, straight catenary action and curved catenary action are developed in PC and RC specimens, respectively. **Fig. 20** illustrates the comparison of the load-displacement curves from PC specimens with bonded strands and counterparts with unbonded strands (PCUSL-0.6 and PCUSH-0.6). The results of PCUSL-0.6 and PCUSH-0.6 had been discussed in authors' previous paper[12]. As shown in Fig. 20, PCUSL-0.6 and PCUSH-0.6 achieve relatively less initial stiffness and yield load comparing to PCSL-0.6 and PCSH-0.6, respectively. However, in catenary actions stage, the ultimate load capacity of PCUSL-0.6 and PCUSH-0.6 are 140 kN (31.5 kip) and 170 kN (38.2 kip), respectively. Thus, PC specimens with unbonded strands are able to mobilize larger catenary action as the stress in unbonded strands are more uniform, which prevents premature fracture of the strands in catenary action stage. Due to spacing limiting, the effects on bonding of strands on horizontal reaction force and failure modes are not discussed herein.

CONCLUSIONS

Based on the results of this experimental investigation, the following conclusions are drawn:

1. Different to conventional RC frames, post-tensioning concrete (PC) frames has little benefits from compressive arch action to prevent progressive collapse. However, the stretching of bonded post-tensioning tendons (BPT) could provide additional vertical load resistance from the beginning of the test. However, the BPT will not detriment the deformation capacity of the frames and thus, the catenary action attributed to both non-prestressed reinforcements and BPT, which could provide reliable second defense line for progressive collapse prevention. BPT could increase the yield load and ultimate capacity of corresponding RC counterpart up by 48% and 131%, respectively.
2. Test results indicated that higher initial effective prestress in the BPT will increase the yield load capacity of the PC frame slightly, but not the ultimate load capacity. Analytical analysis and test results revealed that the ultimate load capacity of the PC frame is dependent on the amount of BPT and non-prestressed reinforcement ratio, rather than the initial effective prestress in the BPT. Inversely, the potential of earlier fracture of BPT raised by high initial effective prestress in the tendon should be taken enough attentions.
3. Based on the test results, it is found that the RCLL with larger span/depth ratio of 14 will reduce the yield load and ultimate load capacity by 22% and 34%, respectively. However, PCLL-0.6 with larger span/depth ratio 14 only decreases the yield load and ultimate load capacity of PC frames only by 12% and 18%, respectively. Thus, the span/depth ratio has less effect on PC frames than RC frames.
4. The amount of non-prestressed reinforcement could improve the capacity of PC frames to resist progressive collapse, including yielding and ultimate load capacities.

Further studies should be conducted to capture the optimal ratio of prestressed reinforcement to non-prestressed reinforcements for optimal resilience performance.

FUTURE RESEARCH

As the loss of column is instantaneous due to blast or vehicular impact, further research studies are needed on dynamic performance of prestressed concrete frames subjected to sudden column removal scenario. Moreover, more studies should be carried out by including the impact effects of disaster such as fire and blast impact or pressure.

ACKNOWLEDGMENTS

This research was supported by a research grant provided by the Natural Science Foundation of China (Nos.51778153, 51568004, 51478118). Any opinions, findings and conclusions expressed in this paper do not necessarily reflect the view of Natural Science Foundation of China.

REFERENCES

1. ASCE/SEI 7, "Minimum Design Loads for Buildings and Other Structures," Structural Engineering Institute-American Society of Civil Engineers, Reston, VA, 2010, 424 pp.

2. Su, Y. P., Tian, Y., and Song, X. S., "Progressive Collapse Resistance of Axially-Restrained Frame Beams," *ACI Structural Journal*, V. 106, No. 5, July-Aug. 2009, pp. 600-607.

3. Orton, S., Jirsa, J. O., and Bayrak, O., "Carbon Fiber-Reinforced Polymer for Continuing in Existing Reinforced Concrete Buildings Vulnerable to Collapse," *ACI Structural Journal*, V. 106, No. 5, July-Aug. 2009, pp. 608-616.

4. Yu, J., and Tan, K. H., "Experimental and Numerical Investigation on Progressive Collapse Resistance of Reinforced Concrete Beam Column Sub-assemblages," *Engineering Structures*, V.55, 2013, pp. 90-106.

5. Sasani, M., and Kropelnicki, J., "Progressive Collapse Analysis of an RC Structure," *The Structural Design of Tall and Special Buildings,* V. 17, No. 4, 2008, pp.757-771.

6. Lew, H. S., Bao, Y. H., Pujol, S., and Sozen, M. A., "Experimental Study of Reinforced Concrete Assemblies under Column Removal Scenario," *ACI Structural Journal,* V.111, No.4, 2014, pp. 881-892.

7. Qian, K. and Li, B., "Slab Effects on the Response of Reinforced Concrete Substructures after Loss of Corner Column." *ACI Structural Journal,* V.109, No. 6, 2012, pp. 845-855.

8. Dat, P. X., and Tan, K. H., "Experimental Study of Beam-Slab Substructures subjected to a Penultimate-Internal Column Loss," *Engineering Structures*, V.55, 2013, pp. 2-15.

9. Ren, P. Q., Li, Y., Lu, X. Z., Guan, H., and Zhou, Y. L., "Experimental Investigation of Progressive Collapse Resistance of One-Way Reinforced Concrete Beam-Slab Substructures under a Middle-Column-Removal Scenario," *Engineering Structures,* V.118, July 2016, pp. 28–40.

10. Qian, K., Li, B., and Zhang, Z., "Influence of Multicolumn Removal on the Behavior of RC Floors," *Journal of Structural Engineering,* V. 142, No. 5, May 2016, 04016006.

11. Peng, Z. H., Orton, S. L., Liu, J. R., and Tian, Y., "Experimental Study of Dynamic Progressive Collapse in Flat-Plate Buildings subjected to Exterior Column Removal," *Journal of Structural Engineering,* V. 143, No. 9, Sep. 2017, 04017125.

12. Qian, K., Yi, Liu, Tao, Y., and Li, B., "Progressive Collapse Resistance of Post-Tensioned Concrete Beam-Column Sub-assemblages with Un-Bonded Post-Tensioning Strands," *Journal of Structural Engineering*, V.144, No. 1, Jan.-2018, 04017182.

13. Kim, J., and Choi, H., "Monotonic Loading Tests of RC Beam-Column Subassemblage Strengthened to Prevent Progressive Collapse," *International Journal of Concrete Structures and Materials*, V.9, No.4, 2015, pp. 401-413.

14. GSA, "Progressive Collapse Analysis and Design Guidelines for New Federal Office Buildings and Major Modernization Projects," *U.S. General Service Administration*, Washington, DC, 2010.

15. DoD, “Design of Building to Resist Progressive Collapse,” Unified Facility Criteria, UFC 4-023-03, *U.S. Department of Defense*, Washington, DC, 2005.

16. ACI Committee 318, “Building Code Requirements for Structural Concrete (ACI 318-14) and Commentary (318R-14),” American Concrete Institute, Farmington Hills, MI, 2014, 433 pp.

17. Izzuddin, B. A., Vlassis, A. G., Elghazouli, A. Y., and Nethercot, D. A., “Progressive Collapse of Multi-Storey Buildings due to Sudden Column Loss—Part Ⅰ: Simplified Assessment Framework,” *Engineering Structures*, V. 30, No. 5, 2008, pp. 1308-18.

18. Tsai, M. H. and Lin, B. H., “Investigation of Progressive Collapse Resistance and Inelastic Response for an Earthquake-Resistant RC Building Subjected to Column Failure.” *Engineering Structures,* V. 30, 2008, pp. 3619–3628.

19. Qian, K., and Li, B., "Research Advances in Design of Structures to Resist Progressive Collapse." *Journal of Performance of Constructed Facilities,* ASCE, 29(5), 2015, B4014007.

20. Yi, W., He, Q., Xiao, Y., and Kunnath, S. K. “Experimental Study on Progressive Collapse-Resistant Behavior of Reinforced Concrete Frame Structures.” *ACI Structural Journal*, 105(4), 2008, pp. 433-439.

TABLES AND FIGURES

List of Tables:

List of Figures:

Fig. 16 – Strain gauge results of PCSL-0.6: (a) top non-prestressed rebar; (b) bottom non-prestressed rebar; (c) prestressed tendon

Fig. 17 – Dynamic performance of the specimens

Fig. 18 – The relationship of internal forces and the load resistance

Fig. 19 – Resistance contributions from axial and shear force (a) RCSL, (b) PCSL-0.6, (c) PCSH-0.6

Fig. 20 – Bonding effects on load-displacement curves

Table 1-Specimen properties

Test ID	Beam Clear Span mm (in.)	Diameter of Post-tensioning Strands mm (in.)	Effective Prestress	Effective Prestress after Loss	Top (Bottom) Beam Long. Rebar Ratio ρ	Axial Force in the Center Column kN (kip)
RCSL	2750 (108.3)	N/A	N/A	N/A	0.7% (0.7%)	-25 (-5.6)
RCLL	3300 (129.9)	N/A	N/A	N/A	0.7% (0.7%)	-30 (-6.7)
PCSL-0.6	2750 (108.3)	12.7 (0.5)	0.6 f_{pu}	0.53 f_{pu}	0.7% (0.7%)	-25 (-5.6)
PCSL-0.75	2750 (108.3)	12.7 (0.5)	0.75 f_{pu}	0.71 f_{pu}	0.7% (0.7%)	-25 (-5.6)
PCSH-0.6	2750 (108.3)	12.7 (0.5)	0.6 f_{pu}	0.54 f_{pu}	1.0% (1.0%)	-25 (-5.6)
PCLL-0.6	3300 (129.9)	12.7 (0.5)	0.6 f_{pu}	0.55 f_{pu}	0.7% (0.7%)	-30 (-6.7)

Note: reinforcement ratio were determined using equation $\rho = A_s/bd_0$, in which b and d_0 represent the width and the effective depth of beam cross sections; f_{pu} is the ultimate strength of the strands.

Table 2-Material properties of reinforcement and unbonded post-tensioning strands

Items		Nominal Diameter mm (in.)	Yield Strength MPa (ksi)	Ultimate Strength MPa (ksi)	Elongation (%)
Transverse Reinforcement	R6	6 (0.24)	372 (54)	510 (74)	19.5
Longitudinal Reinforcements	T10	10 (0.39)	455 (66)	635 (92)	22.8
Post-tensioning Strands		12.7 (0.5)	1650 (239)	1860 (270)	6.1

Notes: R6 represents plain bar of with diameter of 6 mm (0.24 in.); T10 represents deformed rebar with diameter of 10 mm (0.39 in.), respectively.

Table 3-Test results

Specimen ID	Critical Displacements, mm (in.)				Critical Loads, kN (kip)			MHTF kN (kip)	MPF kN (kip)
	RAF	YL	FPL	UL	YL	FPL	UL		
RCSL	34 (1.3)	40 (1.6)	67 (2.6)	598 (23.5)	32 (7.2)	44 (9.9)	68 (15.3)	153 (34.3)	N/A
RCLL	59 (2.3)	46 (1.8)	80 (3.1)	413 (16.3)	25 (5.6)	36 (8.1)	45 (10.1)	135 (30.3)	N/A
PCSL-0.6	20 (0.8)	41 (1.6)	N/A	621 (24.4)	42 (9.4)	N/A	127 (28.5)	291 (65.4)	192 (43.1)
PCSH-0.6	14 (0.6)	43 (1.7)	N/A	613 (24.1)	55 (12.3)	N/A	145 (32.6)	321 (72.1)	186 (41.8)
PCSL-0.75	19 (0.7)	40 (1.6)	N/A	575 (22.6)	46 (10.3)	N/A	117 (26.3)	265 (59.6)	187 (42.0)
PCLL-0.6	33 (1.3)	45 (1.9)	N/A	625 (24.6)	37 (8.5)	N/A	104 (23.4)	280 (62.9)	182 (40.9)

Note: RAF represents releasing axial force completely; YL means yielding load capacity; FPL represents first peak load; UL represents ultimate load capacity; MHTF means maximum horizontal tensile force; and MPF represents maximum prestressing force.

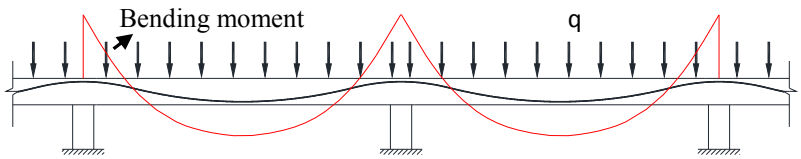

(a)

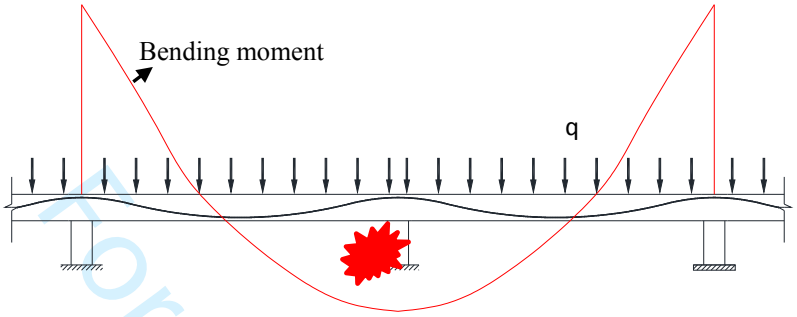

(b)

Fig. 1–Bending moment of the PC sub-frame: (a) before removal of the middle column; and (b) after removal of the middle column

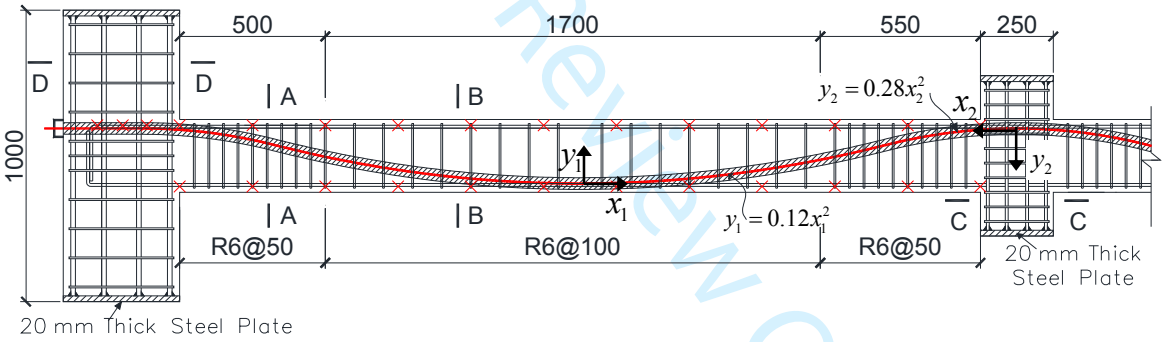

(a)

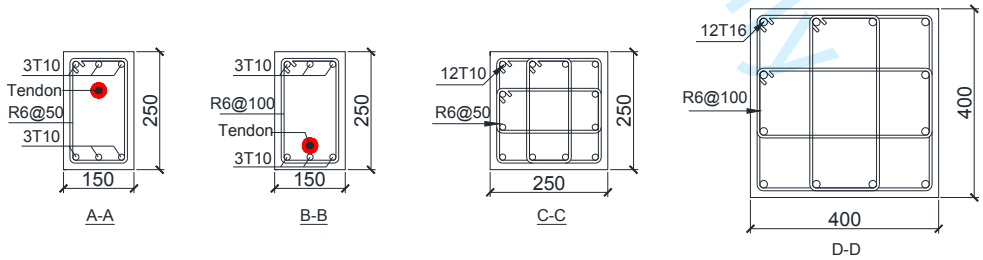

(b)

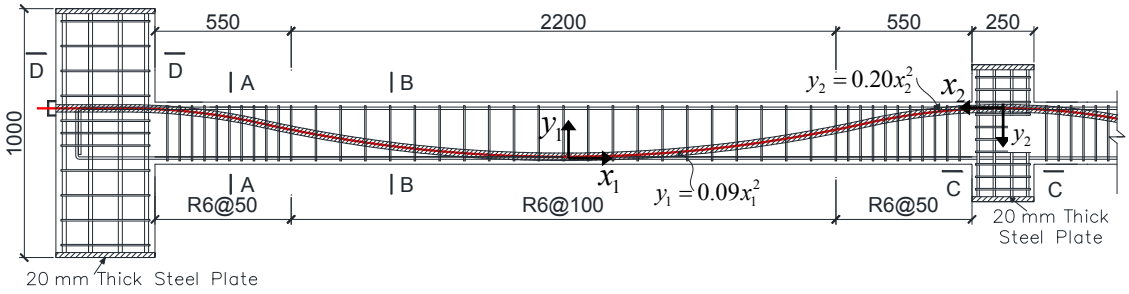

(c)

Fig. 2–Dimensions and reinforcement details: (a) Specimen PCSL-06; (b) cross sections; and (c) Specimen PCLL-0.6

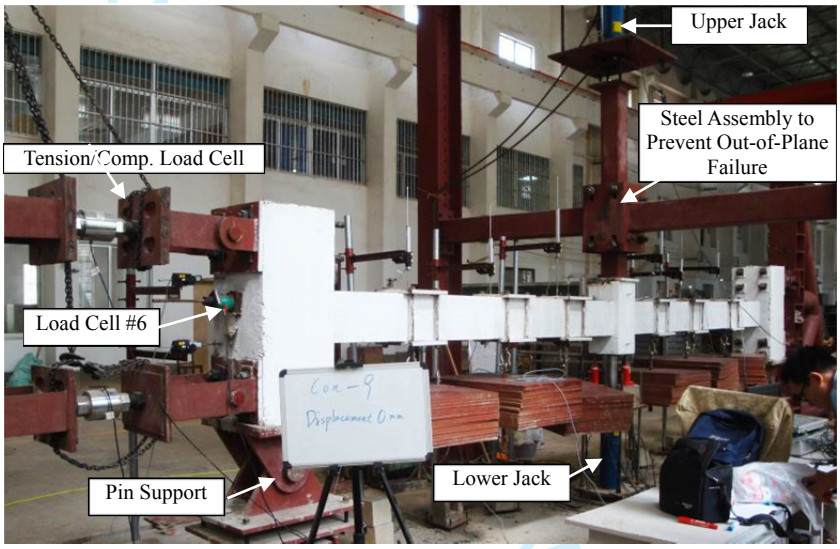

(a)

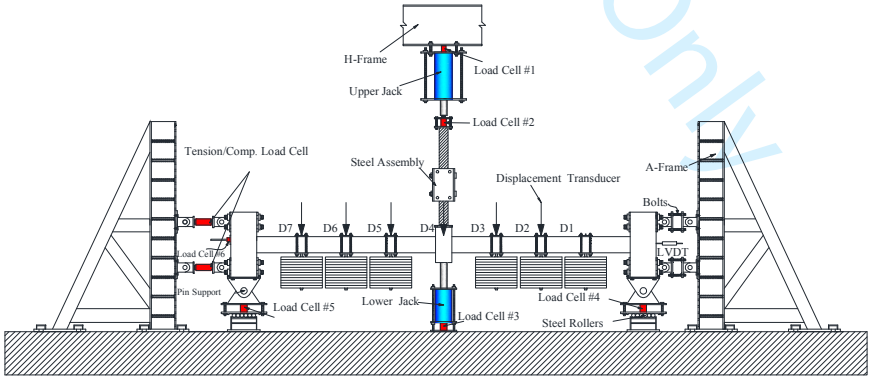

(b)

Fig. 3– Test setup and instrumentation layout of the tests: (a) Setup; (b) Instrumentation layout

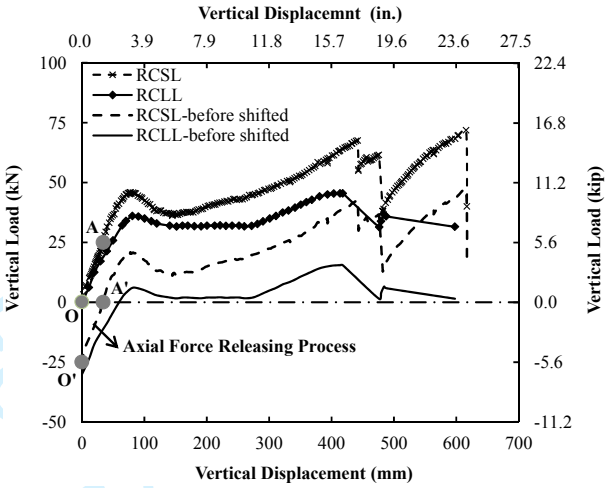

(a)

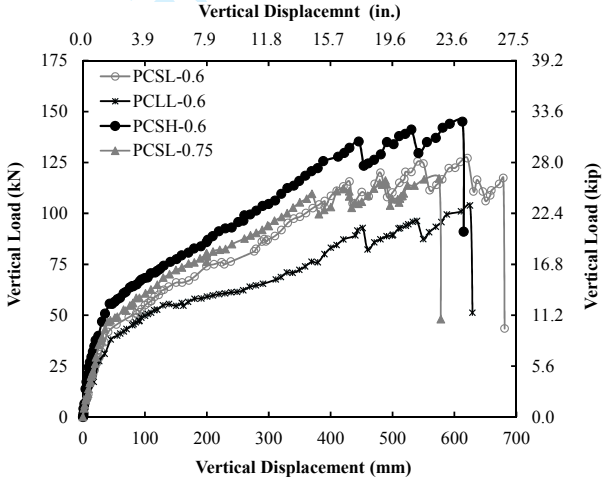

(b)

Fig. 4– Load-displacement history: (a) RC specimens; (b) PC specimens

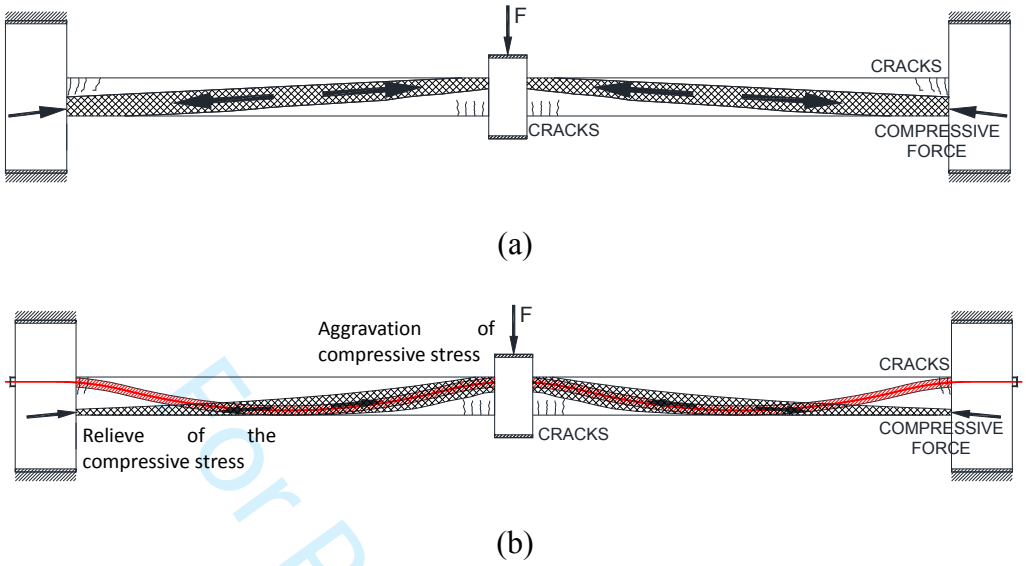

Fig. 5– Schematic of the compressive arch action: (a) RC specimen; (b) PC specimen

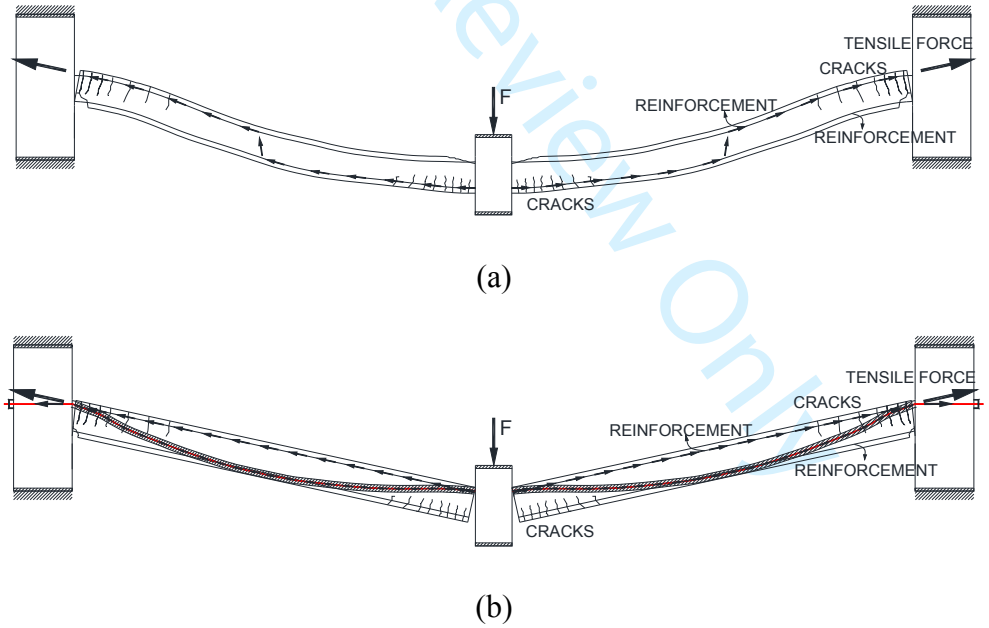

Fig. 6– Schematic of the catenary action: (a) RC specimen; (b) PC specimen

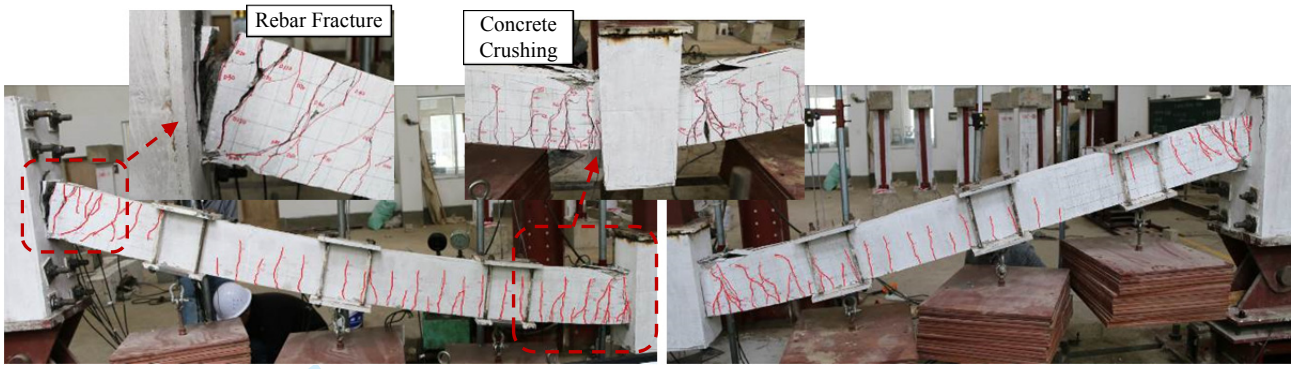

(a)

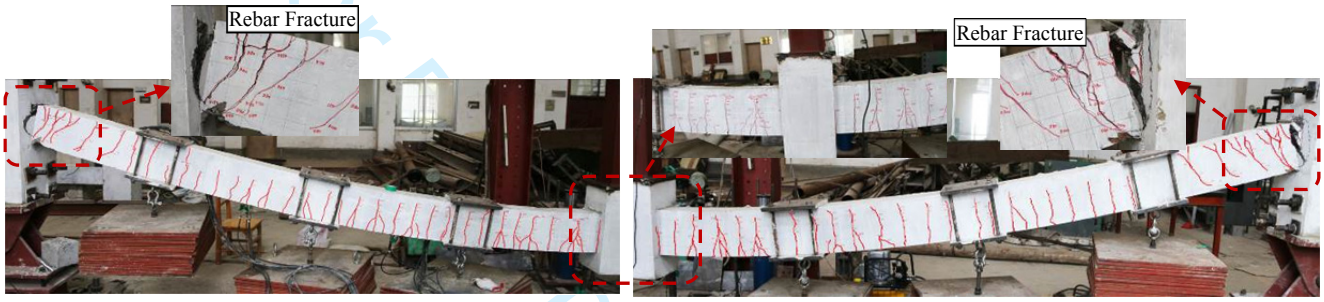

(b)

Fig. 7– Failure mode of controlled RC specimens: (a) RCSL; (b) RCLL

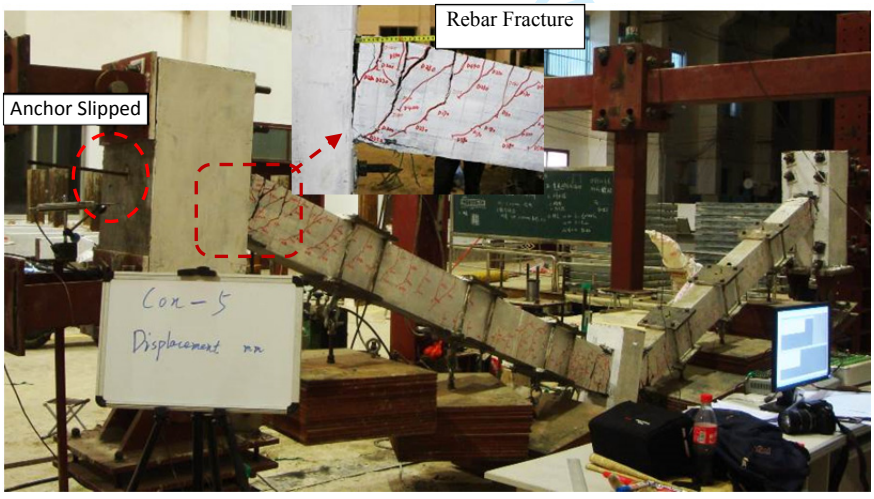

Fig. 8– Failure mode of PC specimen PCSL-0.6

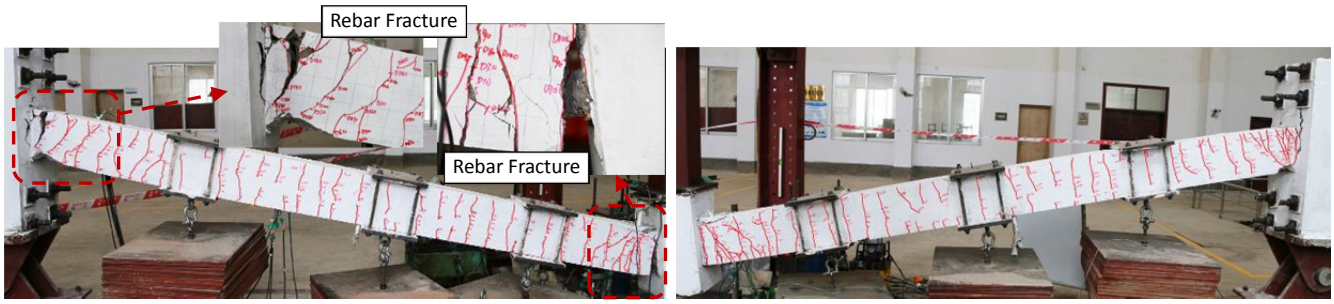

Fig. 9– Failure mode of PC specimen PCLL-0.6

Fig. 10– Failure mode of PC specimen PCSH-0.6

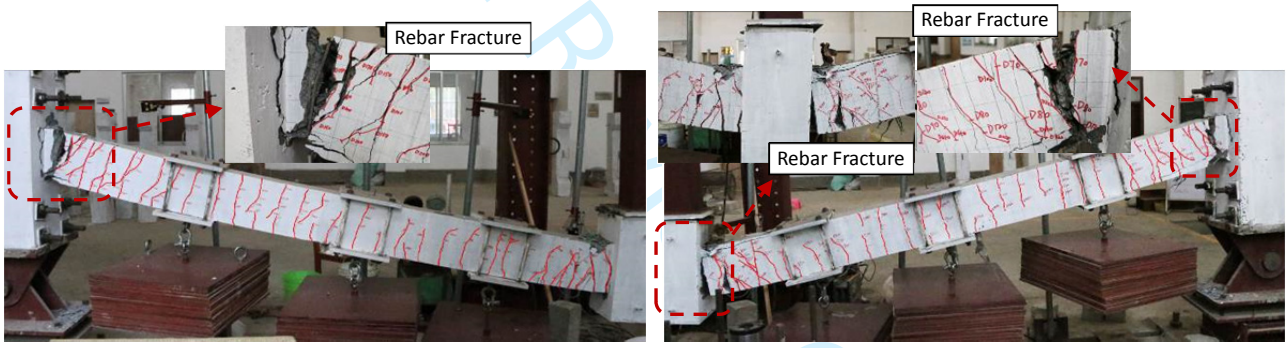

Fig. 11– Failure mode of PC specimen PCSL-0.75

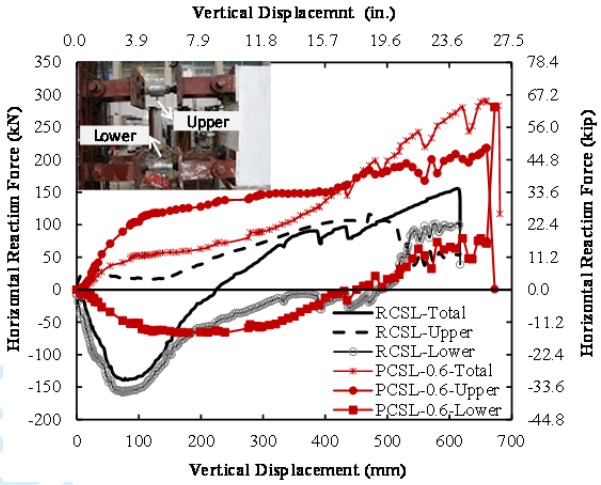

Fig. 12–Horizontal reaction force of lower and upper roller

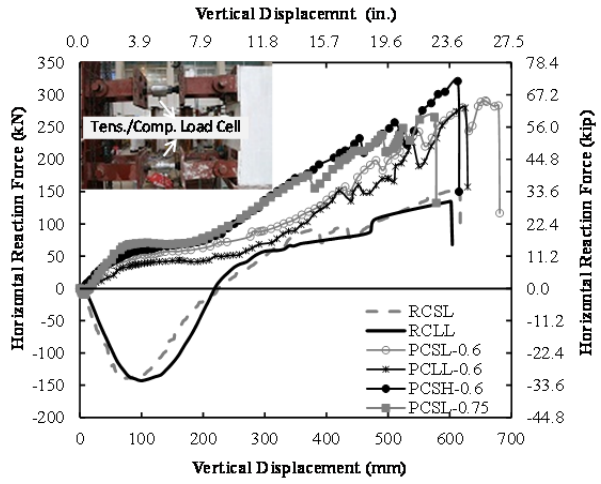

Fig. 13– Comparison of the horizontal reaction force-displacement history

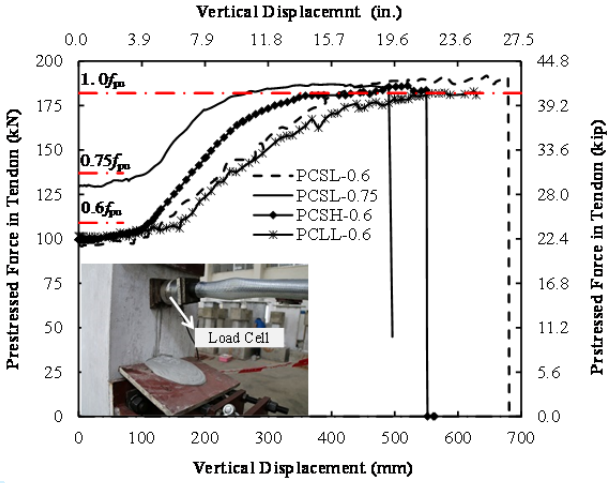

Fig. 14– Prestressed force in the tendon of all specimens

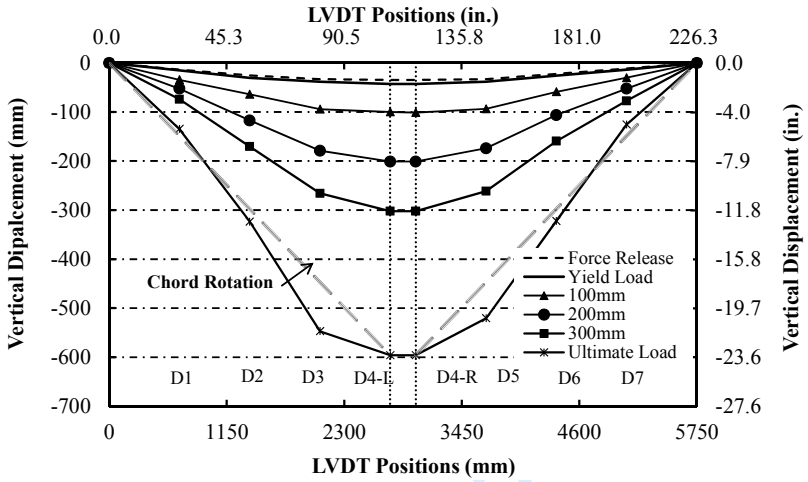

(a)

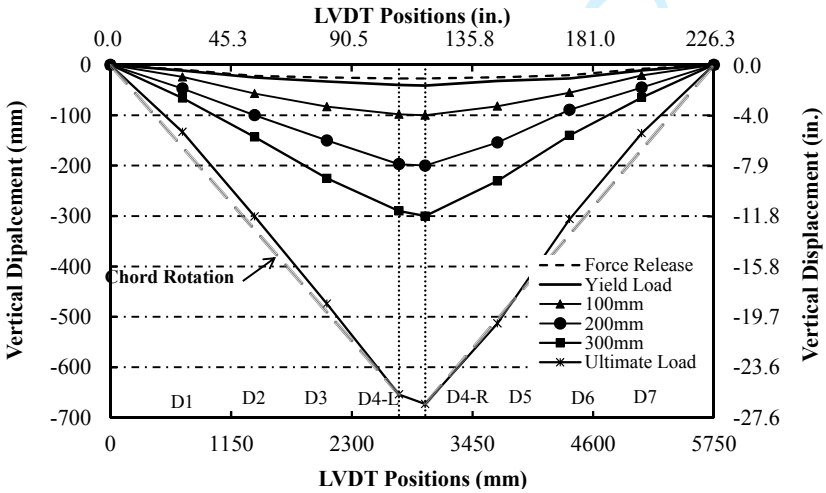

(b)

Fig. 15– Deformation shape of test specimens: (a) RCSL; (b) PCSL-0.6

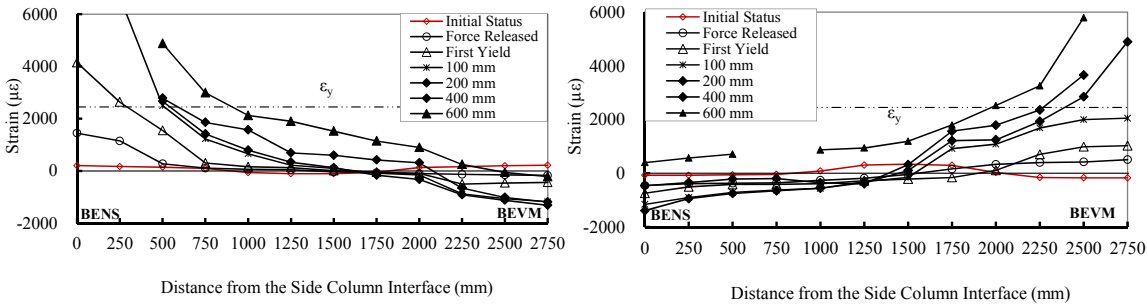

(a) (b)

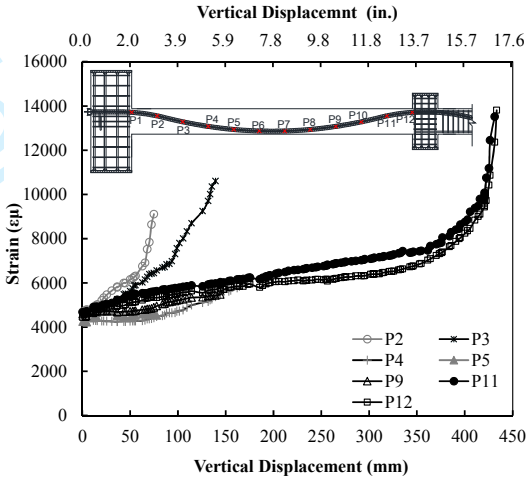

(c)

Fig. 16– Strain gauge results of PCSL-0.6: (a) top non-prestressed rebar; (b) bottom non-prestressed rebar; (c) prestressed tendon

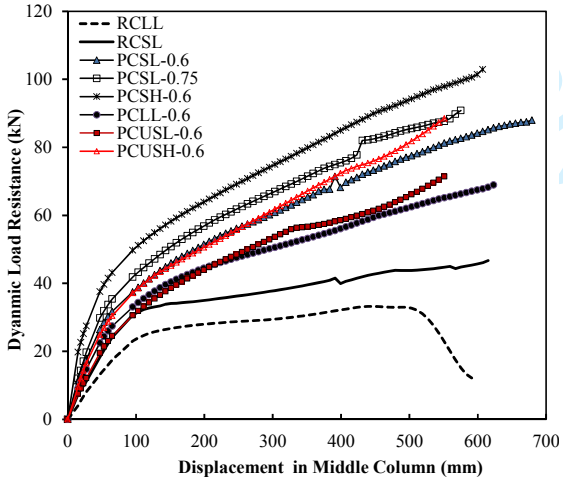

Fig. 17– Dynamic performance of the specimens

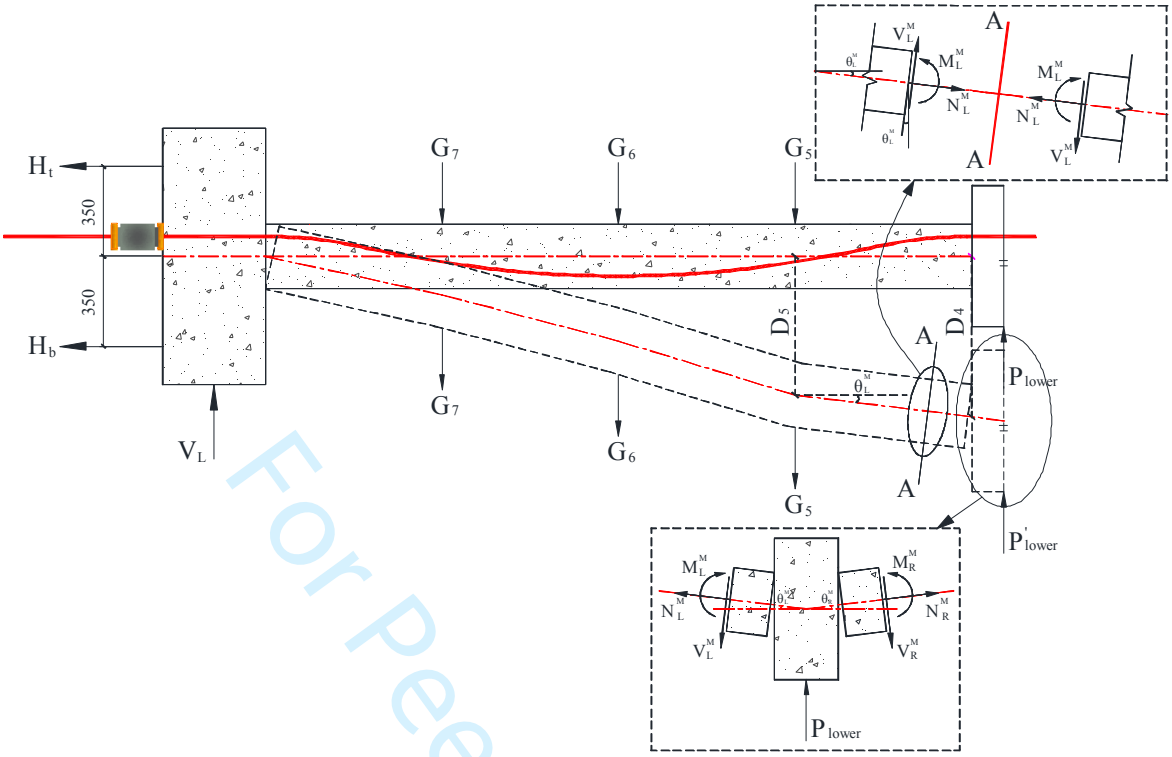

Fig. 18– The relationship of internal forces and the load resistance

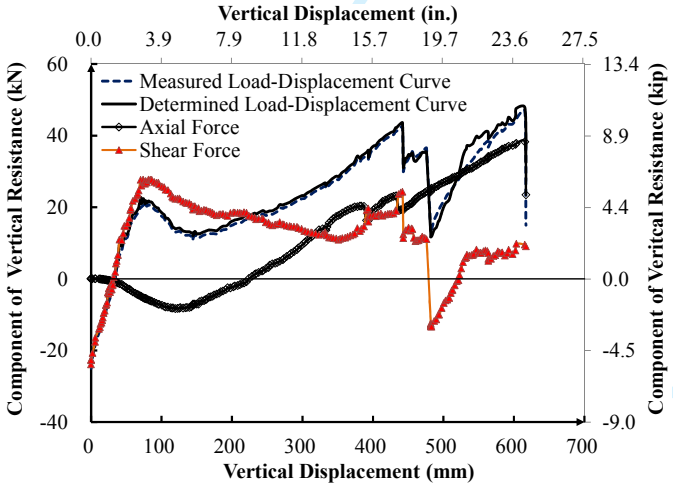

(a)

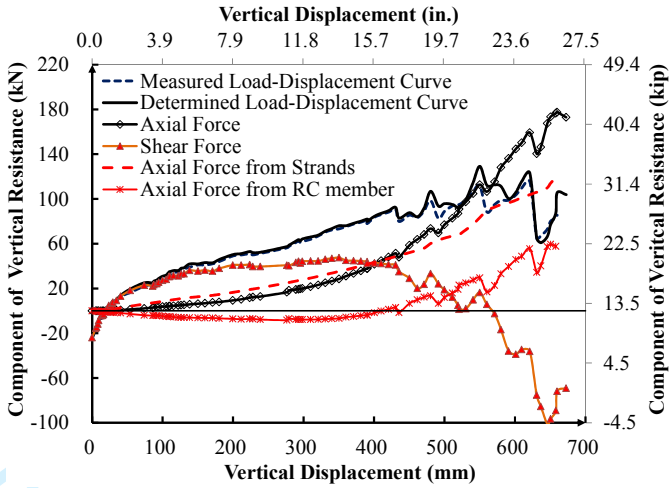

(b)

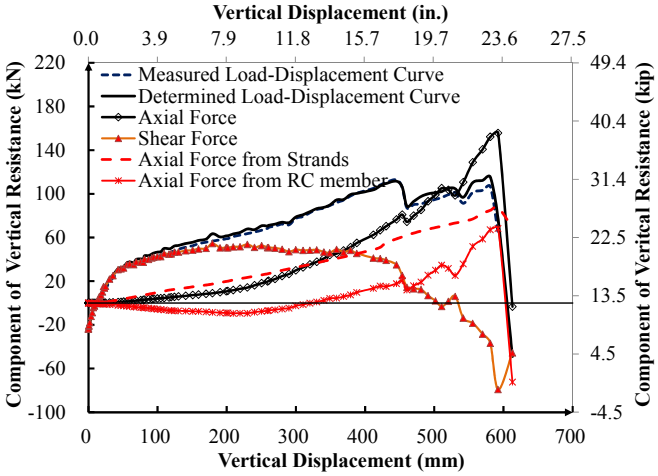

(c)

Fig. 19– Resistance contributions from axial and shear force (a) RCSL, (b) PCSL-0.6, (c) PCSH-0.6

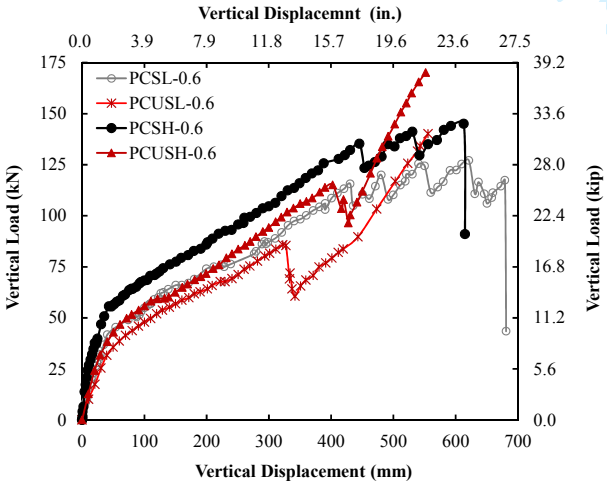

Fig. 20– Bonding effects on load-displacement curves